IMPACT: International Journal of Research in Engineering & Technology (IMPACT: IJRET)
ISSN(E): 2321-8843; ISSN(P): 2347-4599
Vol. 2, Issue 3, Mar 2014, 173-184

PV/BATTERY TO THE GRID INTEGRATION OF HYBRID ENERGY CONVERSION SYSTEM WITH POWER QUALITY IMPROVEMENT ISSUES

P. MOHAN[1], G. S. SUGANYA[2] & T. SIVANANDHAN[3]

[1,2]PG Student, Department of Electrical and Electronics Engineering, Sapthagiri College of Engineering, Anna University, Chennai, Tamil Nadu, India

[3]UG Student, Department of Electrical and Electronics Engineering, Sapthagiri College of Engineering, Anna University, Chennai, Tamil Nadu, India

ABSTRACT

Grid integration of photo voltaic (PV)/Battery hybrid energy conversion system with (i) multi-functional features of micro grid-side bidirectional voltage source converter (μGVSC) (ii) tight voltage regulation capability of battery converter (iii) MPPT tracking performance of high gain integrated cascaded boost (HGICB) dc-dc Converter with quadratic gain and less current ripple are presented in this paper. The PV side HGICB Converter is controlled by P&O MPPT algorithm to extract the maximum power from the variable solar irradiation. This paper proposes a modified Instantaneous symmetrical components theory to the μG-VSC in micro-grid applications with following intelligent functionalities (a) to feed the generated active power in proportional to irradiation levels into the grid (b) compensation of the reactive power, (c) load balancing and (d) mitigation of current harmonics generated by non-linear loads, if any, at the point of common coupling (PCC), thus enabling the grid to supply only sinusoidal current at unity power factor.

The battery energy storage system (BESS) is regulated to balance the power between PV generation and utility grid. A new control algorithm is also proposed in this paper for the battery converter with tight DC link voltage regulation capability. The dynamic performance of battery converter is investigated and compared with conventional average current mode control (ACMC). A model of a hybrid PV Energy Conversion System is developed and simulated in MATLAB/SIMULINK environment. The effectiveness of the proposed control strategies for HGICB converter and μG-VSC with battery energy conversion system are validated through extensive simulation studies.

KEYWORDS: PV Energy Conversion System, High Gain Integrated Cascaded Boost DC-DC Converter, Instantaneous Symmetrical Components Theory, Battery Energy Storage System

1 INTRODUCTION

Among various renewable energy resources, PV and wind power are most rapidly growing renewable energy sources [1]. The PV source is a nonlinear energy source and direct connection of load will not give optimum utilization of the PV system. In order to utilize the PV source optimally, it is necessary to provide an intermediate electronic controller in between source and load under all operating conditions [2]. Using this electronic controller it is possible to operate the PV source at maximum power point (MPP), thus improving the energy efficiency of the PV system. Many control algorithms have been reported in the literature to track maximum power from the PV arrays, such as incremental conductance (INC), constant voltage (CV), and perturbation and observation (P&O). The two algorithms often

used to achieve maximum power point tracking are the P&O and INC methods [2], [3]. Many DC-DC converter topologies are available to track the MPP in PV generating system. Cascade connection of Conventional converters provides wider conversion ratios [4]. One of the major advantages of these converters is a high gain and low current ripple.

However, this configuration has a drawback that the total efficiency may become low if the number of stages is high, owing to power losses in the switching devices [4]. A quadratic converter configuration is also available that uses single switch and achieves quadratic gain [4]. An interesting attractive converter topology is a high gain integrated cascaded boost converter having n-converters connected in cascade using a single active switch.

The instability caused by the cascade structure is avoided, when compared with the conventional cascade boost converter [4]. This class of converters can be used only when the required number of stages is not very large, else the efficiency will be reduced. However, this class of converters for PV applications is not reported in the technical literature. Micro-grid power converters can be classified into (i) grid feeding,(ii) grid-supporting, and (iii) grid-forming power Converters [5]. There are many control schemes reported in the literature such as synchronous reference theory, power balance theory, and direct current vector control [6], [7], for control of μG-VSC in micro grid application. This algorithm requires complex coordinate transformations, which is cumbersome.

Compared to the control strategies mentioned above, the Instantaneous symmetrical component based control proposed in this paper for micro-grid applications is simple in formulation, avoids interpretation of instantaneous reactive power and needs no complex transformations. This paper is structured as follows: In section 2, system description and modeling of various components are presented. The proposed control strategies for HGICB DC-DC Converter, Battery Converter and μG-VSC are discussed in section 3. The simulation results are presented in section 4. With Concluding remarks in section 5.

2 SYSTEM DESCRIPTIONS

The envisaged system consists of a PV/Battery hybrid System with the main grid connecting to non-linear and Unbalanced loads at the PCC as shown in the Figure 1. The photovoltaic system is modeled as nonlinear voltage sources [8]. The PV array is connected to HGICB dc-dc converter and bidirectional battery converters are shown in Figure 1, which are coupled at the dc side of a μG-VSC. The HGICB dc - dc converter is connected to the PV array works as MPPT Controller and battery converter is used to regulate the power flow between dc and ac side of the system.

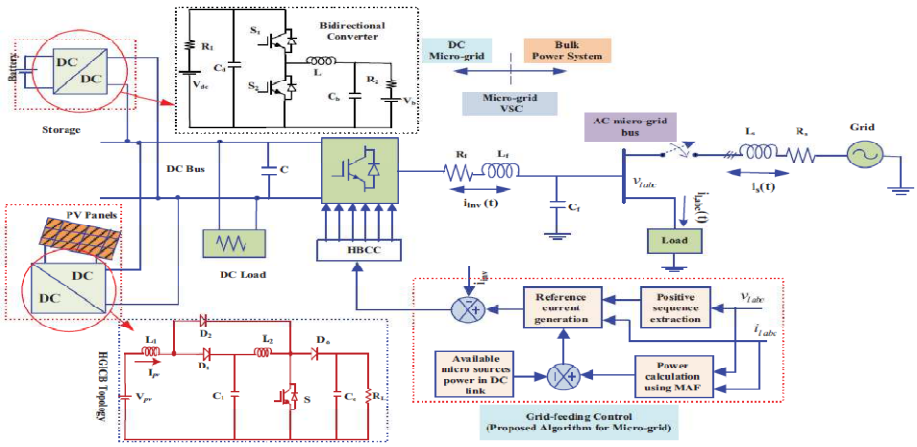

Figure 1: Hybrid Energy Conversion System under Consideration

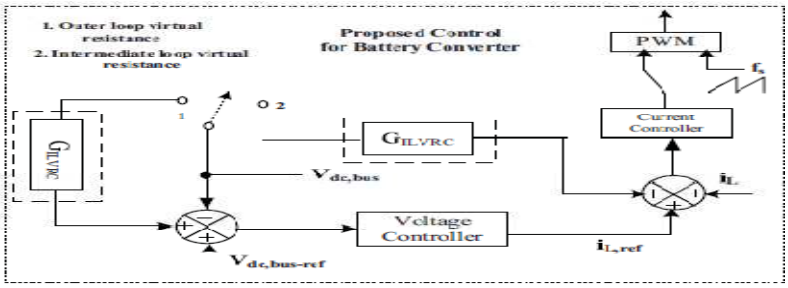

Figure 2: A New Modified-ACMC Control Strategy for Battery Converter

3 MODELING AND CONTROL

The MPPT algorithm for HGICB Converter, control approaches for battery converter and μG-VSC are discussed in the following sections.

3.1 PV Array Model

The mathematical model of PV system referred in [8] is used in this work.

3.2 Battery Converter Modeling

The battery converter goes through two topological stages in each switching period, its power stage dynamics can be described by a set of state equations. The average state space model of the converter can therefore be given as:

$$\frac{di_L}{dt} = \frac{v_{c1}\, d_{(t)}}{L} - \frac{v_{c2}}{L} - \frac{(r_s + r_L) i_L}{L} \quad (1)$$

$$\frac{dv_{c1}}{dt} = \frac{vdc_{,bus} - Vc1}{C_1 R_1} - \frac{iLd_{(t)}}{C_1}$$

$$\frac{dv_{c2}}{dt} = \frac{v_B - v_{c2}}{C_2 R_2} - \frac{i_L}{C_2}$$

The averaged model is nonlinear and time-invariant because of the duty cycle, d(t). This model is finally linearized about the operating point to obtain a small-signal model is shown in Figure 4. The following are the important transfer functions used to design the compensators and to analyze the system behavior under small signal conditions (i) the duty-cycle-to output transfer function $G_{cv}(s)$, carries the information needed to determine the type of the voltage feedback compensation,(ii) the duty-cycle-to-inductor current transfer function $G_{ci}(s)$, is needed to determine the current controller structure.

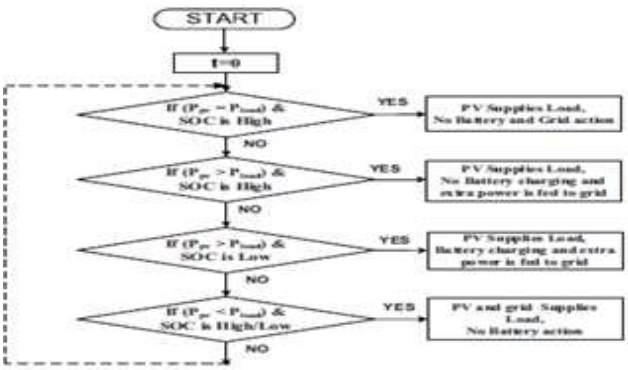

Figure 3: Flow Chart of Power Flow in Hybrid System

4 PROPOSED CONTROL FOR BATTERY CONVERTER

If AC side of μG-VSC has constant power appliances (CPAs), in the small-signal sense, CPAs nature leads to negative incremental input-conductance which causes destabilization of the dc-link voltage [10]. On the micro grid generation side, the inherent negative admittance dynamics of their controlled conversion stages challenges the dc-link voltage control and stability. This effect is more with reduced dc-link capacitance. Therefore, in both cases, fast and effective control and stabilization of the dc-link voltage is very crucial issue. To address this problem, many methods are reported in the literature like (i) by large DC link capacitance (ii) by adding passive resistances at various positions in DC LC filter (iii) by loop cancellation methods [9], [10]. In this paper, a new modified-ACMC (MACMC) control algorithm is proposed for effective control and stabilization of battery converter by introducing virtual resistance (VR) in the (i) outer loop called outer loop virtual resistance control (OLVRC) (ii) intermediate loop called inner loop virtual resistance control (ILVRC) as shown in Figure 2. The proposed virtual resistance based dynamic damping methods aim at injecting a damping signal that compensate for negative conductance caused by CPAs without any power loss.

4.1 Design Steps for Compensators of BESS

The effectiveness of proposed VRCs control algorithm is investigated and compared with the use of traditional ACMC [11]. The flowchart for modes of operation of battery converter in grid-feeding mode is shown in Figure 3. The design guidelines for inner and outer loop compensators of ACMC are given below. The inner loop (current) gain can be written as:

$$T_{i(s)=} G_{id}(s) R_i G_{ci}(s) F_m \quad (2)$$

The outer loop (voltage) gain can be written as:

$$T_{v(s)=} G_{vd}(s) G_{cv}(s) \left(1 + G_{ci}(s)\right) F_m \quad (3)$$

And the overall loop gain therefore can be written as,

$$T_1(s) = Ts + T_v$$

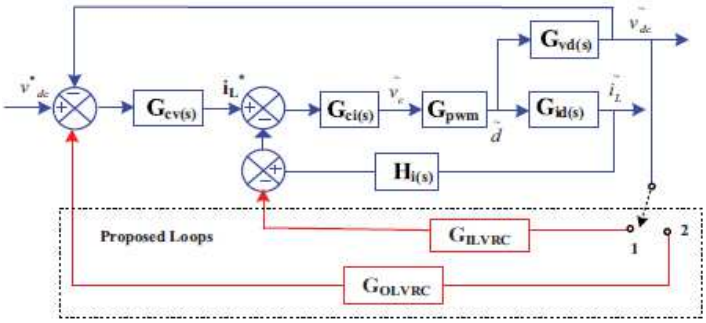

Figure 4: Inner and Outer Loops of Battery Converter with MACMC

Voltage Loop Design Steps:

- Place one zero as high as possible, yet not exceeding resonating frequency of the converter.
- Place one pole at frequency of output capacitor ESR to cancel the effects of output capacitor ESR.
- Adjust, gain of compensator to trade-off stability margins and closed-loop performance.

- Another pole should be place at origin to boost the dc and low frequency gain of the voltage loop.

Similar steps mentioned above are followed to design current loop and for design of MACMC loops. Following the design procedure given above, the inner current and outer voltage loop compensators are designed to regulate the DC link Voltage to 920 V.

5 GENERATION OF REFERENCE CURRENTS FOR µG-VSC

The main aim of the µG-VSC control is to cancel the effects of unbalanced and harmonic components of the local load, while supplying pre-specified amount of real and reactive powers to the load. Upon successfully meeting this objective, the grid current ig will then be balanced and so will be the PCC voltage v_p provided, grid voltage v_g is balanced. Let us denote the three phases by the subscripts a, b and c. Since i_g is balanced, we can write:

$$i_{ga} + i_{gb} + i_{gc} = 0. \quad (5)$$

From the Figure 1, Kirch offs current law (KCL) at PCC gives

$$i_{g,abc} + i_{inv,abc} = i_{L,abc.} \quad (6)$$

Therefore, from (5) and (6), we can write as:

$$i_{inv,a} + i_{inv,b} + i_{inv,}c = i_{L,a} + i_{L,b} + i_{L,c}. \quad (7)$$

Since i_g is balanced due to the action of the compensator, the voltage v_p will also become balanced. Hence, the instantaneous real powers P_g will be equal to its average component. Therefore, we can write

$$P_g = v_{pa}\, i_{ga} + v_{pb}\, i_{gb} + v_{pc}\, i_{gc} \quad (8)$$

Table 1: System Parameters

System Quantities	Values
System voltages	325 V peak phase to neutral, 50 Hz
Linear Load	$Z_{la} = 50 + j1.57\ \Omega$, $Z_{lb} = 45 + j3.14\ \Omega$, $Z_{lc} = 40 + j4.71\ \Omega$
Non Linear Load	Three phase full bridge rectifier load feeding a R-L load of 44Ω-3 mH
G-VSC parameters	C_{dc}=660 μF, V_{dcref}=920 V, L_f= 5 mH, R_f= 0.1Ω
Hysteresis band	0.25 A

Solving above equations, the µG-VSC reference currents are obtained as follows:

$$\begin{aligned} i^*_{inv,a} &= i_{la} - \frac{v_{ga} + \beta(v_{gb} - v_{gc})}{\Delta}(P_{lavg} - P_{\mu s} + P_{loss}) \\ i^*_{inv,b} &= i_{lb} - \frac{v_{gb} + \beta(v_{gc} - v_{ga})}{\Delta}(P_{lavg} - P_{\mu s} + P_{loss}) \\ i^*_{inv,c} &= i_{la} - \frac{v_{gc} + \beta(v_{ga} - v_{gb})}{\Delta}(P_{lavg} - P_{\mu s} + P_{loss}) \end{aligned} \quad (9)$$

where,

$$\Delta = \sum_{j=a,b,c} v_{gj}^2, \beta = tan\varphi/\sqrt{3} = \frac{Q_s}{P_s\sqrt{3}}.$$

and $Q_s = Q_l - Q_{\mu s}$, and by substituting $\beta P_s = \frac{Q_s}{\sqrt{3}}$ into the equation (9), the modified G-VSC reference current equations in terms of active and reactive components are obtained as:

$$i^*_{inv,a} = i_{la} - \frac{v_{ga} P_s}{\sum_{j=a,b,c} v^2_{gj}} - \frac{(v_{gb} - v_{gc}) Q_s}{\sum_{j=a,b,c} v^2_{gj}\sqrt{3}}$$
$$i^*_{inv,b} = i_{lb} - \frac{v_{gb} P_s}{\sum_{j=a,b,c} v^2_{gj}} - \frac{(v_{gc} - v_{ga}) Q_s}{\sum_{j=a,b,c} v^2_{gj}\sqrt{3}}$$
$$i^*_{inv,c} = i_{lc} - \frac{v_{gc} P_s}{\sum_{j=a,b,c} v^2_{gj}} - \frac{(v_{ga} - v_{gb}) Q_s}{\sum_{i=a,b,c} v^2_{gi}\sqrt{3}} \quad (10)$$

In equations (9) and (10), $P_{\mu s}$, P_{lavg}, and Q_l are the available micro source power, average load power, and load reactive power respectively. P_{loss} denotes the switching losses and ohmic losses in actual compensator. The term P_{lavg} is obtained using a moving average filter of one cycle window of time T in seconds.

6 RESULTS AND DISCUSSIONS

The proposed control strategies for PV hybrid generating system is developed and simulated using Matlab/SIMULINK under different solar isolation levels. In order to capture the transient response of the proposed control system, PV isolation is assumed to increase from 200 to 1000 W/m^2 at 0.3 s, and decreases from 1000 to 200 W/m^2 at 0.5 s. This abrupt increase or decrease is assumed in this work in order to test the robustness of the proposed control algorithm. As a result, the inductor current of the HGICB converter is varied to track the maximum power accordingly and the power flow between the μG-VSC, grid and load is also varied under above the operating conditions.

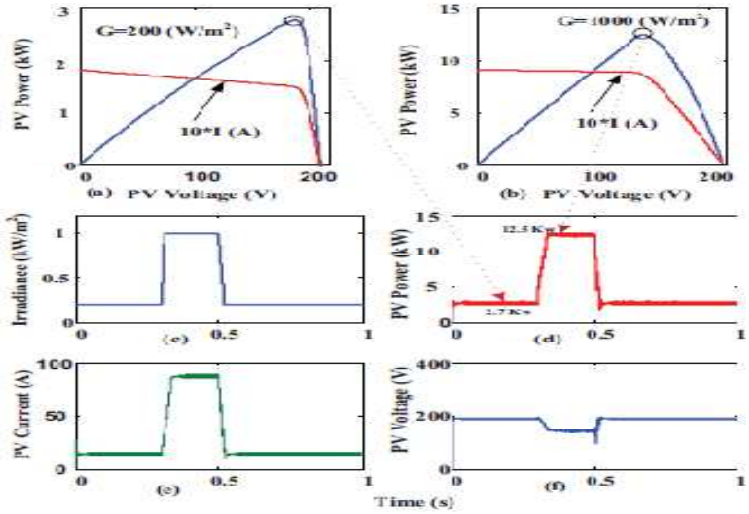

Figure 5: Simulation Results: MPPT Tracking Performance of HGICB Converter (a) PV Characteristic at G=200 *W/m²* (b) PV Characteristic at G=1000 *W/m²* (c) Insolation Variations (d) Maximum Power (e) PV Current (f) PV Voltage

Table 2: Maximum Power Tracking Performance

Time (s)	G (W/m^2)	V_{puref} (V)	I_{puref} (A)	P_{pumax} (kW)
0.2 – 0.3	200	190	14	2.5
0.3 – 0.5	1000	142	87	12.5
0.5 – 1	200	190	14	2.5

5.1 MPPT Tracking Performance of HGICB Converter

The dynamic performance of HGICB converter with P&O MPPT algorithm at two different isolation levels are shown in Figure 5. A variable PV voltage and current in proportion to isolation levels are applied to HGICB converter and as a result, the duty cycle is calculated using the MPPT algorithm. The PV characteristics at two isolation levels are shown in Figure 5(a)-(b). From Figure 5 (a), the maximum power, current and voltage are 2.6kW, 14A and 190V respectively and these values are tracked by HGICB converter which are shown in Figure 5 (d)-(f). Tracked values of PV power, voltage and currents are given in Table 2 for the above operating isolation levels. From these results it can be concluded that, HGICB converter is tracking maximum power closely at all operating conditions.

5.2 Performance of MG-VSC with Different Isolation Levels

The µG-VSC is actively controlled to inject the generated active power as well as to compensate the harmonic and reactive power demanded by the unbalanced and non-linear load at PCC, such that the current drawn from grid is purely sinusoidal at UPF. The dynamic compensation performance of µG-VSC using proposed control algorithm with isolation change and non linear unbalanced load currents are shown in the Figure 6 (a)-(d) along with grid side currents.

When isolation = 200 W/m^2, the maximum power extracted from PV arrays is 2.5kW and the total dc load power (4.5 kW) is partly supplied by PV arrays and the remaining dc load power (2 kW) is drawn from grid through the bidirectional µG-VSC. Here observed that the power flows from ac side to dc link as shown in the Figure 7. When isolation G = 1000 W/m^2, the maximum power available from PV arrays is 12.5kW, part of this power (4.5 kW) is supplied to dc load and remaining power (8 kW) is supplied to the ac load through bidirectional µG-VSC. In this case, the power flows from dc link to ac side. This shows the bidirectional power flow capability of µG-VSC. These dynamics of power flows can be seen from Figure 7. The corresponding variations in the grid current against grid voltage with upf are shown in the Figure 8.

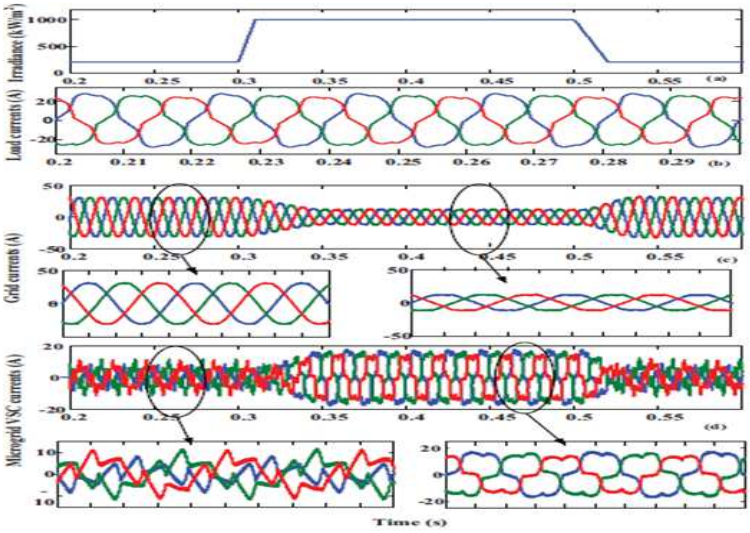

Figure 6: Simulation Results Using Proposed Control Approach for Micro-Grid Side VSC: (a) Insolation Changes (b) Load Currents (c) Grid Currents (d) µG-VSC Currents

µG-VSC using proposed control algorithm with isolation change and non linear unbalanced load currents are shown in the Figure 6 (a)-(d) along with grid side currents. When isolation = 200 W/m^2, the maximum power extracted from PV arrays is 2.5kW and the total dc load power (4.5 kW) is partly supplied by PV arrays and the remaining

dc load power (2 kW) is drawn from grid through the bidirectional μG-VSC. Here observed that the power flows from ac side to dc link as shown in the Figure 7. When isolation G = 1000 W/m^2, the maximum power available from PV arrays is 12.5kW, part of this power (4.5 kW) is supplied to dc load and remaining power (8 kW) is supplied to the ac load through bidirectional μG-VSC. In this case, the power flows from dc link to ac side. This shows the bidirectional power flow capability of μG-VSC. These dynamics of power flows can be seen from Figure 7. The corresponding variations in the grid current against grid voltage with upf are shown in the Figure 8, along with dc link voltage variations.

Table 3

G (W/m^2)	P_{Load} (ac+dc)(kW)	P_{pv} (kW)	P_{inv} (kW)	P_{grid} (kW)
200	13+4.5	2.5	-2	15
1000	13+4.5	12.5	+8	5

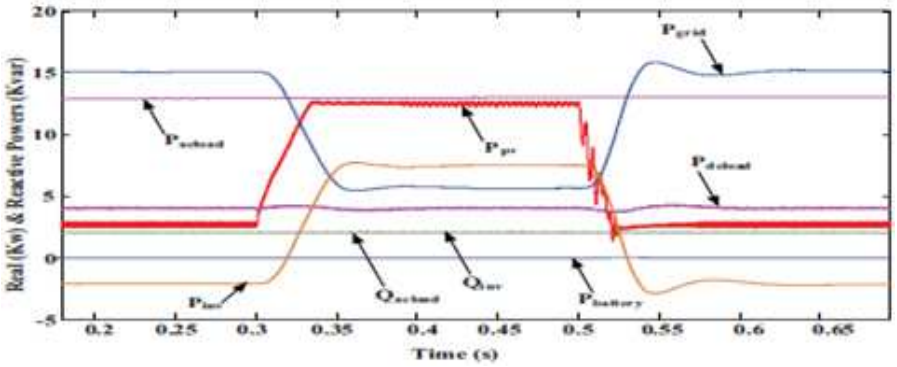

Figure 7: Real and Reactive Power Flow Waveforms of PV Hybrid Generation System

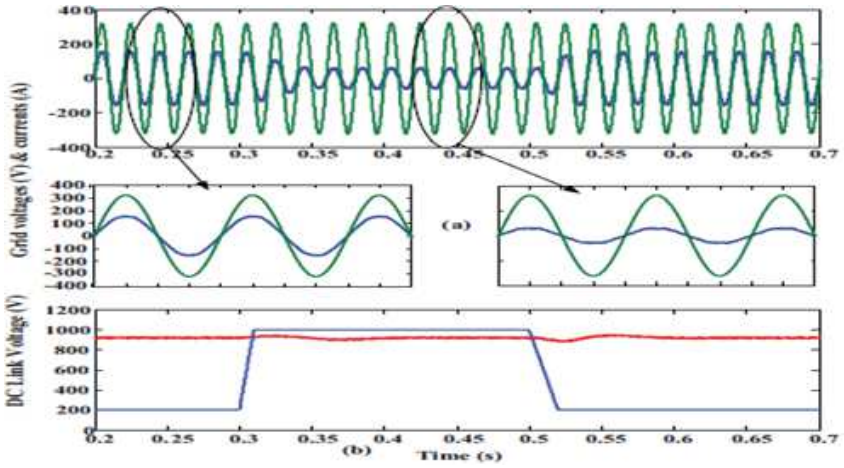

Figure 8: Simulation Results: Performance of Proposed Control Approach
(a) Grid Voltages and Currents (b) DC Link Voltage Dynamics with Different Insolation

5.2 Performance of Battery Converter Control Algorithms with DC Load Variations and Isolation Changes

The dynamic performance of ACMC and MACMC proposed in this paper are investigated through (i) DC load variations (ii) isolation changes. At t=0.35 s, the dc load is changed from 4.5 kW to 5.5 kW. Corresponding to these variations, the DC link voltage regulation capability of these two control algorithms are shown in the Figure 9. From Figure 9, it can be concluded t hat for dc load changes, the modified-ACMC gives better DC Link voltage regulation capability when compared to ACMC. The battery performance with reference to above changes are captured and are shown in the Figure 10.

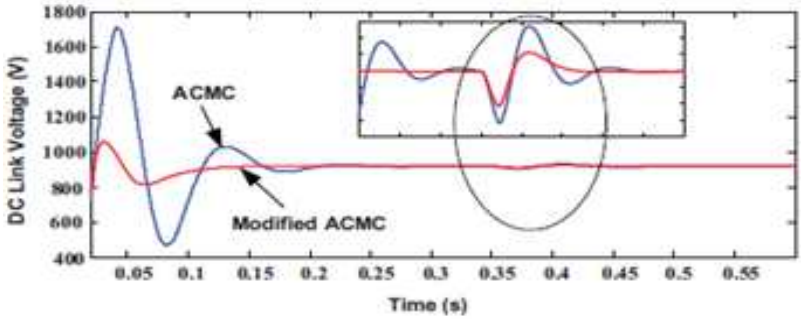

Figure 9: DC Link Voltage Dynamic Using ACMC and MACMC Control Algorithms

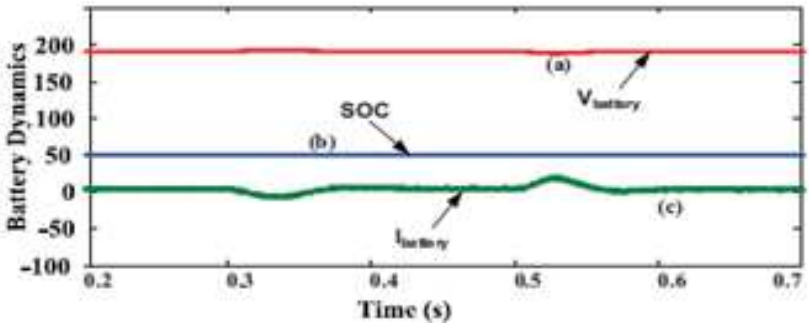

Figure 10: Battery Performance Using Proposed Control Approach to Bidirectional Battery Converter (a) Battery Voltage (b) State of Charge (SOC) (c) Battery Current

6 CONCLUSIONS

The performance of PV/Battery hybrid energy conversion system has been demonstrated with the application of modified Instantaneous symmetrical components theory to μG-VSC proposed in this paper, an efficient control strategy is also proposed for battery converter to regulate the dc bus voltage tightly, under varying solar isolation and dc load conditions. HGICB converter topology is used to track the MPPT with high gain and less current ripple. The μG-VSC is able to inject the generated power into the grid along with harmonic and reactive power compensation for unbalanced non-linear load at the PCC simultaneously. The system works satisfactorily under dynamic conditions. The simulation results under a unbalanced non-linear load with current THD of 12% confirm that the μG VSC can effectively inject the generated active power along with power quality improvement features and thus, it maintains a sinusoidal and UPF current at the grid side with THD of 2.06% (Figure 11).

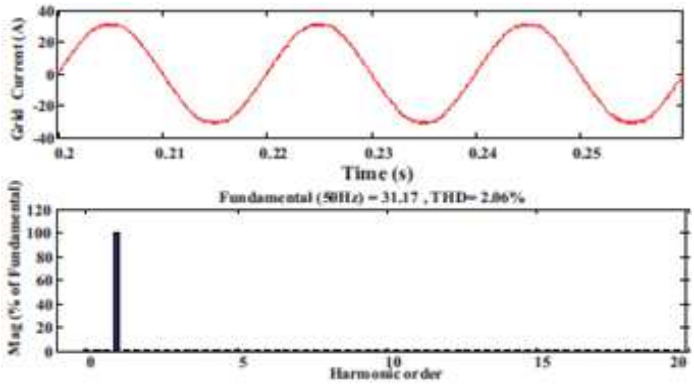

Figure 11: Simulation Results: Performance of Proposed Control Approach (a) Grid Currents (b) Harmonic Spectrum

REFERENCES

1. J. Carrasco, L. Franquelo, J. Bialasiewicz, E. Galvan, R. Guisado, M. Prats, J. Leon, and N. Moreno-Alfonso, "Power-electronic systems for the grid integration of renewable energy sources: A survey," *IEEE Trans. Ind. Electron.*, vol. 53, no. 4, pp. 1002 –1016, Jun. 2006.
2. M. de Brito, L. Galotto, L. Sampaio, G. de Azevedo eMelo, and C. Canesin, "Evaluation of the main mppt techniques for photovoltaic applications," *IEEE Trans. Ind. Electron.*, vol. 60, no. 3, pp. 1156 –1167, Mar. 2013.
3. B. Subudhi and R. Pradhan, "A comparative study on maximum power point tracking techniques for photovoltaic power systems," *IEEE Trans. Sustain. Energy*, vol. PP, no. 99, pp. 1 –10, Mar. 2012.
4. W. Li and X. He, "Review of no isolated high-step-up dc/dc converters in photovoltaic grid-connected applications," *IEEE Trans. Ind. Electron.*, vol. 58, no. 4, pp. 1239 –1250, Apr. 2011.
5. J. Rocabert, A. Luna, F. Blaabjerg, and P. Rodri andguez, "Control of power converters in ac micro grids," *IEEE Trans. Power Electron.*, vol. 27, no. 11, pp. 4734 –4749, Nov. 2012.
6. R. Kadri, J.-P. Gaubert, and G. Champenois, "An improved maximum power point tracking for photovoltaic grid-connected inverter based on voltage-oriented control," *IEEE Trans. Ind. Electron.*, vol. 58, no. 1, pp.66 –75, Jan. 2011.
7. S. Zhang, K.-J. Tseng, D. Vilathgamuwa, T. Nguyen, and X.-Y. Wang, "Design of a robust grid interface system for pmsg-based wind turbine generators," *IEEE Trans. Ind. Electron.*, vol. 58, no. 1, pp. 316–328, Jan. 2011.
8. A. Chatterjee, A. Keyhani, and D. Kapoor, "Identification of photovoltaic source models," *IEEE Trans. Energy Convers.*, vol. 26, no. 3, pp. 883 –889, Sept. 2011.
9. A. Rahimi, G. Williamson, and A. Emadi, "Loop-cancellation technique: A novel nonlinear feedback to overcome the destabilizing effect of constant-power loads," *IEEE Trans. Veh. Technol.*, vol. 59, no. 2, pp.650 –661, Feb. 2010.
10. A. Radwan and Y. Mohamed, "Modeling, analysis, and stabilization of converter-fed ac micro grids with high penetration of converter-interfaced loads," *IEEE Trans. Smart Grid.*, vol. 3, no. 3, pp. 1213 –1225, Sept. 2012.
11. W. Tang, F. Lee, and R. Ridley, "Small-signal modeling of average current-mode control," *IEEE Trans. Power Electron.*, vol. 8, no. 2, pp. 112 –119, Apr. 1993.

AUTHOR'S DETAILS

Mr P Mohan received his BE degree in 1999 from Madras University, Chennai. He received his ME Applied Electronics degree in 2004 from Anna University. He has 11 years of Teaching experience in Electrical and Electronics Engineering in Various Engineering Colleges in Tamilnadu, India. He is currently undergoing ME - Power Systems Engineering degree under Anna University, Chennai. He is Participated in several Conferences, Workshops, Training Programs and Seminars. His areas of Interest are FACTS Devices, Power Electronics, Restructured Power Systems and Renewable Energy Sources.

Miss. G S Suganya received her BE degree in 2012 from Anna University, Chennai. She is undergoing ME - Power Systems Engineering degree under Anna University, Chennai. She is Participated in Conferences, Workshops, Training Programs and Seminars. Her areas of interest are Power Electronics, Power System Operation and Control and State Estimation.

Mr. T Sivanandhan is undergoing BE – Electrical and Electronics Engineering degree Anna University, Chennai. He is Participated in several conferences, Workshops, Training programs and seminars. His areas of Interest are power Electronics, Power Systems Operation and Control and Renewable Energy Sources.